Available online at www.sciencedirect.com
ScienceDirect
International Journal of Heat and Mass Transfer 51 (2008) 1780–1792
International Journal of HEAT and MASS TRANSFER
www.elsevier.com/locate/ijhmt

Mathematical model for gas–liquid two-phase flow and biodegradation of a low concentration volatile organic compound (VOC) in a trickling biofilter

Q. Liao *, X. Tian, R. Chen, X. Zhu

Institute of Engineering Thermophysics, Chongqing University, Chongqing 400044, PR China

Received 18 October 2006; received in revised form 5 July 2007
Available online 5 September 2007

Abstract

A theoretical model is established for predicting the biodegradation of a low concentration volatile organic compound (VOC) in a trickling biofilter. To facilitate the analysis, the packed bed is simplified to a series of straight capillary tubes covered by the biofilm in which the liquid film flow on the surface of biofilm and the gas core flow in the center of tube. The theoretical formulas to calculate liquid film thickness in the capillary tube are obtained by simultaneously solving a set of hydrodynamic equations representing the momentum transport behaviors of the gas–liquid two-phase flow under co-current flow and counter-current flow. Subsequently, the mass transport equations are respectively established for the gas core, liquid film, and biofilm with considering the mass transport resistance in the liquid film and biofilm, the biochemical reaction in the biofilm, and the limitation of oxygen to biochemical reaction. Meanwhile, the surface area of mass transport in the capillary tube is modified by introducing the active biofilm surface area, namely the specific wetted surface area available for biofilm formation. The predicted purification efficiencies of VOC waste gas are found to be in good agreement with the experimental data for the trickling biofilters packed with ∅8 mm, ∅18 mm, and ∅25 mm ceramic spheres under the gas–liquid co-current flow mode and counter-current flow mode. It has been revealed that for a fixed inlet concentration of toluene, the purification efficiency of VOC waste gas decreases with the increase in the gas and liquid flow rate, and increases with the increase in the specific area of packed materials and the height of packed bed. Additionally, it is found that there is an optimal porosity of packed bed corresponding to the maximal purification efficiency.

Keywords: Trickling biofilter; Capillary tube model; Specific wetted surface area of biofilm; Purification efficiency

1. Introduction

In recent years, numerous industrial processes, such as organic chemistry industry, coal industry, rubber regeneration and paint spraying, etc., emit the low concentration volatile organic compounds (VOCs) and the stench gas, which has seriously polluted the atmospheric environment of the local regions. Since the recovery of low concentration VOCs is valueless and its treatment is very difficult and expensive with traditional physical and chemical treatment technologies, the biological treatment technology of VOCs has been more and more extensively applied in the industrial fields because of the high purification efficiency, cost-effectiveness, and environmentally friendliness, etc. The conventional biological reactors for VOCs treatment include biofilters, trickling biofilters, and bioscrubbing filters. It has been proved that trickling biofilters is superior to biofilters when accurate controls of the environmental conditions or higher pollutant elimination rate are required [1]. Besides, trickling biofilters are more recent than biofilters, and have not yet been fully deployed in industrial applications, but the prospective future applications are promising [2]. At present, many researchers have focused

* Corresponding author. Tel./fax: +86 023 65102474.
E-mail address: lqzx@cqu.edu.cn (Q. Liao).

0017-9310/$ - see front matter © 2007 Elsevier Ltd. All rights reserved.
doi:10.1016/j.ijheatmasstransfer.2007.07.007

Nomenclature

A_T	cross-sectional area of the trickling biofilter column, m^2
a	specific surface area of packed material, m^{-1}
a_l	specific active biofilm surface area of trickling biofilter, m^{-1}
C_{bO}	concentration of oxygen in biofilm, g/m^3
C_{bT}	concentration of pollutant in biofilm, g/m^3
C_{gO}	concentration of oxygen in gas phase, g/m^3
C_{gT}	concentration of pollutant in gas phase, g/m^3
C_{lO}	concentration of oxygen in liquid film, g/m^3
C_{lT}	concentration of pollutant in liquid film, g/m^3
D_{bO}	diffusion coefficient of oxygen in biofilm, m^2/s
D_{bT}	diffusion coefficient of pollutant in biofilm, m^2/s
D_{lO}	diffusion coefficient of oxygen in liquid film, m^2/s
D_{lT}	diffusion coefficient of pollutant in liquid film, m^2/s
D_p	diameter of ceramic spheres, m
D_T	diameter of trickling biofilter, m
g	acceleration of gravity, $m\ s^{-2}$
h	height of packed bed, m
K_{IT}	self-inhibition kinetic constant for biodegradation of pollutant, g/m^3
K_O	kinetic constant for biodegradation of oxygen, g/m^3
K_T	kinetic constant for biodegradation of pollutant, g/m^3
m	Henry's constant
n_c	number of capillary tubes
Pe	Peclet number
p_c	capillary pressure, Pa
p	static pressure of gas and liquid in capillary tube, Pa
Q	volume flow rates in trickling biofilter, m^3/h
q	volume flow rates in capillary tube, m^3/s
r_b	radius at the interface of biofilm and liquid film in capillary tube, m
r_l	radius at the interface of gas–liquid in the capillary tube, m
r_s	radius of the capillary tube, m
u	velocity in the capillary tube, m/s
Y_T	dry density of biofilm, kg/m^3
Y_T	yield coefficient of a culture on pollutant

Greek symbols

β	dimensionless number, $\beta_i = X_V \mu_{max} r_S^2/(Y_T D_{bi} C_{gi,in})$, $i = T, O$
ε	porosity of packed bed in the trickling biofilter
η	purification efficiency of the trickling biofilter
μ	dynamic viscosity, $N\ S/m^2$
μ_{max}	maximum specific growth rate of microorganism, h^{-1}
ρ	density, kg/m^3
σ_l	liquid surface tension, N/m
σ_p	surface tension of packing material, N/m
ξ	correction factor

Superscript

*	dimensionless number

Subscripts

b	biofilm
g	gas phase
in	inlet of the trickling biofilter
l	liquid film

on understanding biofiltration process through theoretical models [3–6]. The first and simple model by Ottengraf and van den Oever [3] described kinetics of the elimination processes. Hodge and Devinny [4] proposed a biofiltration model to simulate the basic transport and biological processes of ethanol reduction and subsequent CO_2 formation in columns containing compost, granular activated carbon, or a mixture of compost and diatomaceous earth. Deshusses et al. [5] established a novel diffusion reaction model for the determination of both the steady-state and transient-state behavior of biofilters for waste air biotreatment.

However, the theoretical research work on the trickling biofilters is limited, most of which take no account of the mass transport resistance in the liquid film over the porous material of the packed bed. Baltzis et al. [7,8] developed a transient model and steady model. In the model, general mixing, oxygen limitation aspects, multi-component adsorption phenomena, Monod- and Andrews-type kinetics with interference between the components were considered with respect to not only single components biodegradation but also multi-component biodegradation. The model accounted of the absorption of pollutant at the gas–liquid interface with Henry's law but neglected the mass transport resistance in the liquid film.

A few models involve the effect of mass transport resistance in the liquid film on the biodegradation of pollutant. Among these models, Sun et al. [9] theoretically studied the axial dispersion, convection film mass-transfer, and biodegradation coupled with deactivation of the TCE-degrading enzyme. Mirpuri et al. [10] developed a predictive model to the degradation of toluene in a flat-plate vapor phase bioreactor (VPBR). The VPBR model incorporated kinetic, stoichiometric, injury, and irreversible loss coefficients from suspended culture studies for the toluene degradation by P. Putida 54G and measured values of Henry's law constant and boundary layer thickness at the gas–liquid and liquid–biofilm interface. Alonso et al. [11] established a model by considering a two-phase system,

quasi-steady-state processes, uniform bacterial population, and one limiting substrate. However, it should be noted here that in the aforementioned models, the liquid film thickness was generally evaluated by experience and the pollutant concentration was treated as a constant in the liquid film; the mass transport resistance of the liquid film was simplified as an absorption resistance at gas–liquid interface calculated by Henry's law with a measured Henry constant.

The objective of this work is to propose a new theoretical model of the gas–liquid two-phase flow and biodegradation for the waste gas treatment in the trickling biofilter based on the previous work [12], which considers the effect of pollutant absorption at the gas–liquid interface, mass transfer resistance in liquid film, the diffusion of VOC pollutant and oxygen in biofilm, and biochemical reaction. For assessing the required liquid film thickness over the porous material, the velocity distribution in the liquid film and the gas core under co-current flow and counter-current flow were obtained by solving a set of momentum conservation equations of liquid–gas two-phase flow. Simultaneously, the specific wetted surface area of the biofilm was introduced into modifying the surface area of biofilm under the consideration of the active bioreaction area. In order to testify the theoretical model, an experiment was conducted to find the remove efficiency of toluene waste gas in the trickling biofilter with the ceramic spheres. And finally, theoretical prediction was evaluated by the experimental data.

2. Mathematical model

In establishment of the mathematical model reflecting the transport and biodegradation behavior of the trickling biofilter, it is considered that the packed material serves as a support for micro-organisms accompanied with a flowing circulation liquid film at another side. To facilitate the analysis, the packed bed is simplified to a series of straight capillary tubes covered by the biofilm, in which the liquid is drained downward by the gravity and the waste gas is forced to move upward under the gas–liquid counter-current flow or move downward under the gas–liquid co-current flow in the trickling biofilter. This method has been conventionally applied in the analysis of the flow behaviors and the boiling heat transfer behaviors in porous medium [13,14]. The schematic of the physical problem is showed in Fig. 1a and b. There are three zones in the capillary tube: the biofilm zone over the tube wall ($r_b \leqslant r \leqslant r_s$), the liquid film zone over the biofilm ($r_l \leqslant r \leqslant r_b$), and the gas core zone in the center of the tube ($0 \leqslant r \leqslant r_l$).

With referring to Ref. [15], the radius of the capillary tube can be expressed as

$$r_s = \frac{2\varepsilon}{a(1-\varepsilon)}. \tag{1}$$

During the steady operation, the thickness of the biofilm equals to 0.1 times the radius of the packed material [16]. Therefore, the thickness of the biofilm should be taken into account in determination of the porosity and specific surface area of packed bed.

The transport and biodegradation process of pollutant in above physical domain can be outlined as that the pollutant in waste gas flowing in the gas core is firstly absorbed at the liquid–gas interface, and then diffused in the liquid film and the biofilm, finally degraded by microorganism in the biofilm. Therefore, the mass transport behavior in the liquid film has a significant effect on the removal of VOC and the liquid film thickness profile should be initially determined by the hydraulic theory of gas–liquid two-phase flow in the trickling biofilter. And then, the mass transport control equations are established in the liquid film and biofilm combined with biochemical reaction, respectively. The VOC concentration in liquid film and biofilm, and the distribution of VOC concentration in the trickling biofilter are solved from these equations, which gives the purification efficiency of pollutant finally. The assumptions in the establishment of the model are as follows: (1) the biofilm is formed on the exterior surface of the packed materials, thus no reaction occurs in the pores of the packed materials; (2) the thickness of the biofilm is necessarily uniformly around the packed materials; (3) the size and distribution of particle in the trickling biofilter

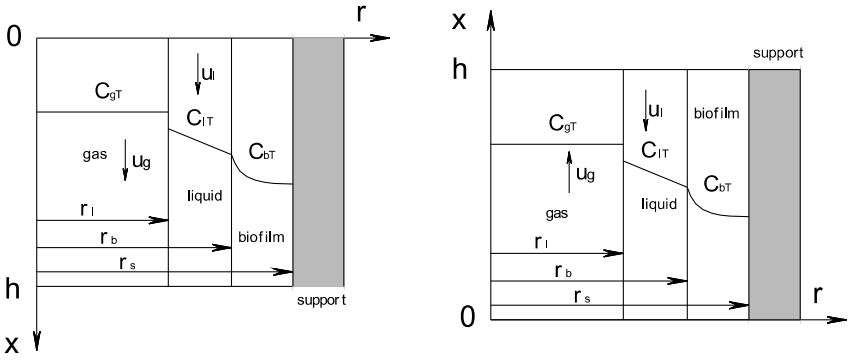

(a) the gas-liquid co-current flow (b) the gas-liquid counter-current flow

Fig. 1. Schematic of the physical model.

is unity; (4) the gas flow and liquid flow are assumed to be one-dimensional fully developed flow in the axial direction of trickling biofilter; (5) the diffusion of the VOC is regarded as being only in the normal direction of the biofilm, i.e. the axial diffusion is neglected; (6) the convective mass transport in the liquid film zone and the VOC concentration difference along the radial direction in the gas core zone are neglected; (7) the absorption of VOC pollutant at the gas–liquid interface can be evaluated with Henry's law; (8) there is no microorganism in the gas core and the liquid film; (9) carbon dioxide and water are the final products of biodegradation.

2.1. Thickness of liquid film

The thickness of liquid film is significantly affected by flow arrangement of gas–liquid two-phase flow. In the next parts, the calculation method of liquid film will be deduced for co-current flow and counter-current flow, respectively.

2.1.1. Gas–liquid co-current flow

The governing conservation equation of momentum in the gas zone ($0 \leqslant r \leqslant r_1$) can be written as

$$\mu_g \frac{1}{r}\frac{d}{dr}\left(r\frac{du_g}{dr}\right) - \frac{dp_g}{dx} = 0 \tag{2}$$

with corresponding boundary conditions for co-current flow

$$r = 0, \quad \frac{du_g}{dr} = 0, \tag{3}$$

$$r = r_1, \quad u_g = u_l, \quad \mu_g \frac{du_g}{dr} = \mu_l \frac{du_l}{dr}, \tag{4}$$

Having a smaller flow rate, the liquid passes through the trickling biofilter in laminar flow. Thus the momentum equation in the liquid film zone is

$$\mu_l \frac{1}{r}\frac{d}{dr}\left(r\frac{du_l}{dr}\right) + \rho_l g - \frac{dp_l}{dx} = 0 \tag{5}$$

with corresponding boundary conditions for co-current flow,

$$r = r_1, \quad u_l = u_g, \quad \mu_l \frac{du_l}{dr} = \mu_g \frac{du_g}{dr}, \tag{6}$$

$$r = r_b, \quad u_l = 0. \tag{7}$$

Simultaneously integrating Eqs. (2) and (5) subject to the boundary conditions (3), (4), (6), and (7), the gas velocity and liquid velocity in the capillary tubes can be deduced as

$$u_g = \frac{1}{4\mu_g}\frac{dp_g}{dx}r^2 + \frac{1}{4\mu_l}\left(\frac{dp_l}{dx} - \rho_l g\right)(r_l^2 - r_b^2) + \frac{r_l^2}{2\mu_l}\left(\frac{dp_g}{dx} - \frac{dp_l}{dx} + \rho_l g\right)\ln\left(\frac{r_l}{r_b}\right) - \frac{1}{4\mu_g}\frac{dp_g}{dx}r_l^2 \tag{8}$$

and

$$u_l = \frac{1}{4\mu_l}\left(\frac{dp_l}{dx} - \rho_l g\right)(r^2 - r_b^2) + \frac{r_l^2}{2\mu_l}\left(\frac{dp_g}{dx} - \frac{dp_l}{dx} + \rho_l g\right)\ln\left(\frac{r}{r_b}\right). \tag{9}$$

The liquid pressure gradient, dp_l/dx, in Eqs. (8) and (9) is related to the gas pressure gradient, dp_g/dx, by the Yang–Laplace equation, as

$$\frac{dp_l}{dx} = \frac{dp_g}{dx} - \frac{dp_c}{dx} = \frac{dp_g}{dx} - \frac{d}{dx}\left(\frac{\sigma_l}{r_l}\right). \tag{10}$$

Then, the flow rates of gas and liquid in the capillary tube for co-current flow are given as

$$\begin{aligned} q_g &= 2\pi\int_0^{r_l} u_g r\,dr \\ &= \frac{\pi}{4\mu_l}\frac{dp_g}{dx}(r_l^4 - r_l^2 r_b^2) - \frac{\pi r_l^4}{8\mu_g}\frac{dp_g}{dx} \\ &\quad - \frac{\pi}{4\mu_l}\left(\frac{dp_c}{dx} + \rho_l g\right)(r_l^4 - r_l^2 r_b^2) \\ &\quad + \frac{\pi r_l^4}{2\mu_l}\left(\frac{dp_c}{dx} + \rho_l g\right)\ln\left(\frac{r_l}{r_b}\right), \end{aligned} \tag{11}$$

$$\begin{aligned} q_l &= 2\pi\int_{r_l}^{r_b} u_l r\,dr \\ &= \frac{\pi}{8\mu_l}\left(\frac{dp_c}{dx} + \rho_l g\right)\left[r_b^4 - 4r_b^2 r_l^2 + 3r_l^4 + 4r_l^4\ln\left(\frac{r_b}{r_l}\right)\right] \\ &\quad - \frac{\pi}{8\mu_l}\frac{dp_g}{dx}(r_b^2 - r_l^2)^2. \end{aligned} \tag{12}$$

By combining Eqs. (10)–(12), the gradient of the radius at the gas–liquid interface, r_l, in the capillary tube is deduced as

$$\frac{dr_l}{dx} = \frac{\pi\rho_l g(A\cdot B - C\cdot D) - 8\mu_l\mu_g q_g C - 8\mu_l q_l B}{\pi A\cdot B - \pi C\cdot D}\cdot\frac{r_l^2}{\sigma_l}, \tag{13}$$

where

$$A = r_b^4 - 4r_l^2 r_b^2 + 3r_l^4 + 4r_l^4\ln\left(\frac{r_b}{r_l}\right), \tag{14}$$

$$B = 2\mu_g(r_l^4 - r_l^2 r_b^2) - \mu_l r_l^4, \tag{15}$$

$$C = (r_b^2 - r_l^2)^2, \tag{16}$$

and

$$D = 2\mu g\left[r_l^4 - r_l^2 r_b^2 - 2r_l^4\ln\left(\frac{r_l}{r_b}\right)\right] \tag{17}$$

with corresponding boundary conditions,

$$x = 0, \quad \boldsymbol{r}_l = \boldsymbol{r}_{l,0}.$$

where $r_{l,0}$ represents the radius at the gas–liquid interface at the liquid entrance of the capillary tube. Due to the larger ratio of height to radius of capillary tube and the lower velocity of gas and liquid flow under consideration in this paper, the liquid flow and the gas flow in capillary tube can be regarded as fully developed flow, approximately,

which implies a constant radius profile, and thus the radius at the liquid–gas interface can be solved from Eq. (13), while letting the left hand side be equal to nil, i.e. $dr_l/dx = 0$, using the Newton iteration method.

2.1.2. Gas–liquid counter-current flow

The governing conservation equation of momentum in the gas zone ($0 \leqslant r \leqslant r_l$) can be written as

$$\mu_g \frac{1}{r}\frac{d}{dr}\left(r\frac{du_g}{dr}\right) - \frac{dp_g}{dx} = 0, \tag{18}$$

with corresponding boundary conditions for the counter-current flow

$$r = 0, \quad \frac{du_g}{dr} = 0, \tag{19}$$

$$r = r_l, \quad u_g = u_l, \quad \mu_g \frac{du_g}{dr} = -\mu_l \frac{du_l}{dr}. \tag{20}$$

The governing conservation equation of momentum in the liquid core zone is

$$\mu_l \frac{1}{r}\frac{d}{dr}\left(r\frac{du_l}{dr}\right) + \rho_l g - \frac{dp_l}{dx} = 0 \tag{21}$$

with corresponding boundary conditions for counter-current flow

$$r = r_l, \quad u_l = u_g, \quad \mu_l \frac{du_l}{dr} = -\mu_g \frac{du_g}{dr}, \tag{22}$$

$$r = r_b, \quad u_l = 0. \tag{23}$$

Simultaneously integrating Eqs. (18) and (21) subject to the boundary conditions (19), (20), (22), and (23), the gas velocity and liquid velocity in the capillary tubes can be deduced as

$$u_g = \frac{1}{4\mu_g}\frac{dp_g}{dx}(r^2 - r_l^2) + \frac{(r_l^2 - r_b^2)}{4\mu_l}\left(\frac{dp_g}{dx} - \frac{dp_c}{dx} - \rho_l g\right) + \frac{r_l^2}{2\mu_l}\left(\frac{dp_c}{dx} - 2\frac{dp_g}{dx} + \rho_l g\right)\ln\left(\frac{r_l}{r_b}\right), \tag{24}$$

and

$$u_l = \frac{1}{4\mu_l}\left(\frac{dp_g}{dx} - \frac{dp_c}{dx} - \rho_l g\right)(r^2 - r_b^2) + \frac{r_l^2}{2\mu_l}\left(\frac{dp_c}{dx} - 2\frac{dp_g}{dx} + \rho_l g\right)\ln\left(\frac{r}{r_b}\right). \tag{25}$$

Then, the flow rate of gas and liquid for counter-current flow yields

$$q_g = \frac{\pi r_l^4}{8\mu_g}\frac{dp_g}{dx} + \frac{\pi}{4\mu_l}\frac{dp_g}{dx}(r_l^4 - r_l^2 r_b^2) - \frac{\pi}{4\mu_l}\left(\frac{dp_c}{dx} + \rho_l g\right)(r_l^4 - r_l^2 r_b^2) + \frac{\pi r_l^4}{2\mu_l}\left(\frac{dp_c}{dx} + \rho_l g\right)\ln\left(\frac{r_l}{r_b}\right) - \frac{\pi r_l^4}{\mu_l}\ln\left(\frac{r_l}{r_b}\right)\frac{dp_g}{dx} - \frac{\pi r_l^4}{4\mu_g}\frac{dp_g}{dx} \tag{26}$$

and

$$q_l = \frac{\pi}{8\mu_l}\left(\frac{dp_c}{dx} + \rho_l g\right)\left[r_b^4 - 4r_b^2 r_l^2 + 3r_l^4 + 4r_l^4 \ln\left(\frac{r_b}{r_l}\right)\right] + \frac{\pi}{8\mu_l}\frac{dp_g}{dx}\left[6r_b^2 r_l^2 - r_b^4 - 5r_l^4 - 8r_l^4 \ln\left(\frac{r_b}{r_l}\right)\right]. \tag{27}$$

Similarly, by combining Eqs. (10), (26) and (27) the gradient of the radius at the gas–liquid interface, r_l, in capillary tube is given as

$$\frac{dr_l}{dx} = \frac{8\mu_l\mu_g q_g C + 8\mu_l q_l B + \pi\rho_l g(C' \cdot D - A \cdot B')}{\pi(C' \cdot D - A \cdot B')}\frac{r_l^2}{\sigma_l}, \tag{28}$$

where

$$B' = 2\mu_g(r_l^4 - r_l^2 r_b^2) + 8\mu_g r_l^4 \ln\left(\frac{r_b}{r_l}\right) - \mu_l r_l^4, \tag{29}$$

and

$$C' = r_b^4 - 6r_b^2 r_l^2 + 5r_l^4 + 8r_l^4 \ln\left(\frac{r_b}{r_l}\right). \tag{30}$$

As mentioned above, the radius at the interface of liquid and gas for counter-current flow can be also solved from Eq. (28) while $dr_l/dx = 0$.

2.2. VOC pollutant transport in the gas core zone, the liquid film zone, and the biofilm zone

From the viewpoints of the biodegradation theory and aforementioned assumptions, the mass transport process of the pollutant and oxygen is considered as consisting of the adsorption at the gas–liquid interface [17], the diffusion in the liquid film, and the diffusion with a biodegradation in the biofilm. As a rule, both the biofilm and the liquid film are very thin and liquid flow is comparatively slow. So, it is considered that the VOC only diffuses in the normal direction of the biofilm and the liquid film, i.e. the axial diffusion and convective transport are neglected in these zones. In addition, the biodegraded behavior of the VOC pollutant by microorganism is evaluated with the Monod- and Andrews-type Kinetics having respect to the limitation of oxygen following the analysis of Zarook and Baltzis [18] for single component biodegradation and multi-component biodegradation. Then, referring to the cylindrical coordinates shown in Fig. 1, the mass conservation equations in the three zones can be written as follows,

(1) Mass conservation equation of the VOC and oxygen in the gas core

$$u_g \frac{dC_{gT}}{dx} - \left.\frac{2D_{lT}}{r_l}\frac{dC_{lT}}{dr}\right|_{r=r_l} = 0, \tag{31}$$

$$u_g \frac{dC_{gO}}{dx} - \left.\frac{2D_{lO}}{r_l}\frac{dC_{lO}}{dr}\right|_{r=r_l} = 0, \tag{32}$$

with corresponding boundary conditions,

$$x = o, \quad C_{gT} = C_{gT,in}, \quad C_{gO} = C_{gO,in}, \tag{33}$$

where C_{gT} and C_{gO} stand for the concentrations of pollutant and oxygen in the gas phase, and C_{lT} and C_{lO} are the concentrations of pollutant and oxygen in the liquid film (g/m^3), respectively. D_{lT} and D_{lO} are the diffusion coefficients of pollutant and oxygen in liquid film (m^2/s), respectively. The subscript "in" represents the parameter at the inlet of the tickling biofilter.

(2) Mass conservation equation of the VOC and oxygen in the liquid film

$$\frac{1}{r}\frac{d}{dr}\left(D_{lT} r \frac{dC_{lT}}{dr}\right) = 0, \tag{34}$$

$$\frac{1}{r}\frac{d}{dr}\left(D_{lO} r \frac{dC_{lO}}{dr}\right) = 0, \tag{35}$$

with corresponding boundary conditions,

$$r = r_l, \quad C_{lT} = \frac{C_{gT}}{m_T}, \quad C_{lO} = \frac{C_{gO}}{m_O}, \tag{36}$$

$$r = r_b, \quad C_{lT} = C_{bT}, \quad C_{lO} = C_{bO},$$

$$D_{lT}\frac{dC_{lT}}{dr} = D_{bT}\frac{dC_{bT}}{dr}, \quad D_{lO}\frac{dC_{lO}}{dr} = D_{bO}\frac{dC_{bO}}{dr}, \tag{37}$$

where m_T and m_O are the Henry's constant of pollutant and oxygen.

(3) Mass conservation equation of the VOC and oxygen in the biofilm

$$D_{bT}\frac{1}{r}\frac{d}{dr}\left(r\frac{dC_{bT}}{dr}\right) = \frac{X_V \mu_{max}}{Y_T}\frac{C_{bT}}{K_T + C_{bT} + (C_{bT}^2/K_{IT})}\frac{C_{bO}}{K_O + C_{bO}}, \tag{38}$$

$$D_{bO}\frac{1}{r}\frac{d}{dr}\left(r\frac{dC_{bO}}{dr}\right) = \frac{X_V \mu_{max}}{Y_T}\frac{C_{bT}}{K_T + C_{bT} + C_{bT}^2/K_{IT}}\frac{C_{bO}}{K_O + C_{bO}}, \tag{39}$$

with corresponding boundary conditions,

$$r = r_s, \quad \frac{dC_{bT}}{dr} = 0, \quad \frac{dC_{bO}}{dr} = 0, \tag{40}$$

where C_{bT} and C_{bO} stand for the concentrations of pollutant and oxygen in the biofilm (kg/m^3), D_{bT} and D_{bO} are the diffusion coefficients of pollutant and oxygen in biofilm (m^2/s); X_V the biofilm dry density (kg/m^3), Y_T the yield coefficient of a culture on pollutant (kg/kg), μ_{max} the constant in the specific growth rate expression, K_T and K_O the kinetic constants for biodegradation of the pollutant and oxygen (g/m^3), and K_{IT} the self-inhibition kinetic constants for biodegradation of the pollutant (g/m^3).

By introducing the following dimensionless parameters:

$$x^* = \frac{x}{h}, \quad r^* = \frac{r}{r_S}, \quad r_L^* = \frac{r_l}{r_S}, \quad r_b^* = \frac{r_b}{r_S}, \quad C_{gT}^* = \frac{C_{gT}}{C_{gT,in}},$$

$$C_{gO}^* = \frac{C_{gO}}{C_{gO,in}}, \quad C_{lT}^* = \frac{C_{lT}}{C_{gT,in}}, \quad C_{lO}^* = \frac{C_{lO}}{C_{gO,in}},$$

$$C_{bT}^* = \frac{C_{bT}}{C_{gT,in}}, \quad C_{bO}^* = \frac{C_{bO}}{C_{gO,in}}, \quad K_T^* = \frac{K_T}{C_{gT,in}},$$

$$K_{IT}^* = \frac{K_{IT}}{C_{gT,in}}, \quad K_O^* = \frac{K_O}{C_{gO,in}}, \quad \phi_T = \frac{D_{bT}}{D_{lT}},$$

and $\quad \phi_O = \frac{D_{bO}}{D_{lO}}$.

Eqs. (31)–(40) can be rewritten in the dimensionless form

$$\frac{dC_{gT}^*}{dx^*} - \frac{2h^2}{Pe_T r_l^* r_s^2}\left.\frac{dC_{lT}^*}{dr^*}\right|_{r^*=r_l^*} = 0, \tag{41}$$

$$\frac{dC_{gO}^*}{dx^*} - \frac{2h^2}{Pe_O r_l^* r_s^2}\left.\frac{dC_{lO}^*}{dr^*}\right|_{r^*=r_l^*} = 0, \tag{42}$$

subject to

$$x^* = 0, \quad C_{gT}^* = 1, \quad C_{gO}^* = 1, \tag{43}$$

$$\frac{1}{r^*}\frac{d}{dr^*}\left(r^*\frac{dC_{lT}^*}{dr^*}\right) = 0, \tag{44}$$

$$\frac{1}{r^*}\frac{d}{dr^*}\left(r^*\frac{dC_{lO}^*}{dr^*}\right) = 0, \tag{45}$$

subject to

$$r^* = r_l^*, \quad C_{lT}^* = \frac{C_{gT}^*}{m_T}, \quad C_{lO}^* = \frac{C_{gO}^*}{m_O}, \tag{46}$$

$$r^* = r_b^*, \quad C_{lT}^* = C_{bT}^*, \quad C_{lO}^* = C_{bO}^*,$$

$$\frac{dC_{lT}^*}{dr^*} = \phi_T\frac{dC_{bT}^*}{dr^*}, \quad \frac{dC_{lO}^*}{dr^*} = \phi_O\frac{dC_{bO}^*}{dr^*} \tag{47}$$

and

$$\frac{1}{r^*}\frac{d}{dr^*}\left(r^*\frac{dC_{bT}^*}{dr^*}\right) = \beta_T\frac{C_{bT}^*}{K_T^* + C_{bT}^* + C_{bT}^{*2}/K_{IT}^*}\frac{C_{bO}^*}{K_O^* + C_{bO}^*}, \tag{48}$$

$$\frac{1}{r^*}\frac{d}{dr^*}\left(r^*\frac{dC_{bO}^*}{dr^*}\right) = \beta_O\frac{C_{bT}^*}{K_T^* + C_{bT}^* + C_{bT}^{*2}/K_{IT}^*}\frac{C_{bO}^*}{K_O^* + C_{bO}^*}, \tag{49}$$

subject to

$$r^* = 1, \quad \frac{dC_{bT}^*}{dr^*} = 0, \quad \frac{dC_{bO}^*}{dr} = 0. \tag{50}$$

In Eqs. (41) and (42), the Peclet number, $Pe_i = u_g h/D_{li}$, $i = T, O$, reflects the ratio of convective mass transport in the gas core zone to molecule diffusion in the liquid film zone, where h is the height of the packed bed. Besides, the dimensionless number β_i, $\beta_i = X_V \mu_{max} r_S^2/(Y_T D_{bi} C_{gi,in})$, $i = T, O$, is introduced into Eqs. (48) and (49).

In addition, the biofilm cannot fully cover the packed material in practice. The surface area of mass transport in the capillary tube is modified through introducing the specific wetted surface area available for biofilm formation. The specific wetted surface area of the biofilm in the trickling biofilter bed, i.e. the area of active biofilm, can be modified via the following equation [7]:

$$\frac{a_l}{\xi a} = 1 - \exp\left\{-1.45\left(\frac{\sigma_p}{\sigma_l}\right)^{0.75}\left(\frac{q_l\rho_l}{A_T a\mu_l}\right)^{0.1}\left(\frac{a}{\rho_l^2 g}\right)^{-0.05} \times \left[\left(\frac{3600 q_l\rho_l}{A_T}\right)^2 \frac{1}{\rho_l\sigma_l a}\right]^{0.2}\right\}, \quad (51)$$

where a_l is the active biofilm surface area per unit volume of the trickling biofilter (m^{-1}), a the total specific surface area of the packing material (m^{-1}), ξ the correction factor, σ_p the surface tension of the packing material (N/m), σ_l the surface tension of liquid (N/m), q_l the liquid flow rate of the trickling biofilter (m^3/s), ρ_l the liquid density (kg/m^3), A_T the cross-sectional area of the trickling biofilter column (m^2), μ_l the liquid viscosity (kg/m s), and g the gravitational acceleration (m/s^2). Finally, the surface area of the biofilm for mass transfer in the model was substituted by the active biofilm surface area. It should be noted that the correction factor, ξ, in Eq. (51) is introduced to consider the effect of liquid–gas flow arrangement and the packed sphere size on the wetted biofilm surface area in the trickling biofilter bed, which was usually adopted by the previous research work for trickling biofilter, for instance, a value of $\xi = 2$ has been reported by Diks and Ottengraf [19,20], and a value of ξ was determined in Mpanias and Baltzis's [7] study to be 4.5, and a value of $\xi = 6$ can be inferred from the results of Pedersen and Arvin [21] who speculated that the enlarged contact area between the air and the biofilm may be due to the irregular surface of the biofilm. The correction factor, ξ, for Eq. (51) is a constant determined by fitting the experimental data of the trickling biofilter with the solutions of the theoretical model for a specific gas–liquid flow arrangement and packed sphere size. The active biofilm surface area per unit volume of the trickling biofilter, a_l, is firstly obtained with the present theoretical model by using the measured purification efficiency, liquid flow rate, and gas flow rate as the known parameters, then the correction factor, ξ, is calculated with Eq. (51) for various liquid flow rates and gas flow rates under the same packed sphere size and gas–liquid flow arrangement, and finally the mean of all the correction factors is treated as the correction factor of this specific packed material and gas–liquid flow arrangement.

The calculation of the concentration distribution of the pollutant and oxygen in the liquid film zone and biofilm zone proceeds in a stepwise manner as follows:

(1) Discretize the terms with the x-derivatives (d/dx) in Eqs. (41) and (42) using the backward finite difference with an increment Δx, and the terms with r-derivatives (d/dr) in Eqs. (44)–(49) with an increment Δr.
(2) Use the concentrations of both pollutant and oxygen at the liquid–biofilm interface and the profiles of pollutant and oxygen concentration in the biofilm based on the inlet condition or the previous axial position x for the subsequent increments are initially utilized to solve the concentration profile of pollutant from Eq. (48) along the r-direction in the biofilm zone and then to solve the concentration profile of oxygen from Eq. (49) by using the solution of the pollutant concentration profile.
(3) Obtain new values of concentrations of pollutant and oxygen in the biofilm from solving Eqs. (48) and (49) using the last solution for concentrations of pollutant and oxygen.
(4) Repeat step (3). The iteration process is terminated when the two successive values of the pollutant and oxygen concentrations in the biofilm agree within a specific tolerance ($\pm 10^{-3}$).
(5) Solve the concentration profiles of pollutant and oxygen in the liquid film zone from Eqs. (44) and (45) based on the concentration profiles of pollutant and oxygen in the biofilm zone.
(6) Calculate the mass fluxes of pollutant and oxygen at the liquid–biofilm interface from the concentration profiles of pollutant and oxygen in the liquid film zone and from the concentration profiles of pollutant and oxygen in the biofilm zone, respectively.
(7) If the discrepancy between the two values of pollutant or oxygen exceeds $\pm 0.1\%$, the new value of pollutant or oxygen concentration at the liquid–biofilm interface is calculated from the average of the two mass fluxes of pollutant or oxygen at the liquid–biofilm interface.
(8) Repeat steps (2)–(7). The iteration process is halted when the two consecutive values of the pollutant or oxygen mass flux at the liquid–biofilm interface agree within a specific tolerance ($\pm 10^{-3}$).
(9) Solve Eqs. (41) and (42) for the pollutant concentration, C^*_{gT}, and the oxygen concentration, C^*_{gO}, in the gas core zone at the next axial position x and then obtain the concentration profiles of pollutant and oxygen along the axial direction with the same aforementioned steps.
(10) The TDMA (Tridiagonal Matrix Algorithm) method is used in the computation process. Finally, the purification efficiency of the trickling biofilter can be obtained from the pollutant concentrations at the inlet and outlet.

3. Experimental apparatus and methods

For testifying the theoretical model, an experiment was conducted for toluene purification with the trickling biofilter. A schematic diagram of the experimental system is presented in Fig. 2. The trickling biofilter was made from stainless steel cylinder with a 0.3 m internal diameter. The height of the trickling biofilter is 1.4 m, and the height of packed bed was 0.5 m. In the experiments for toluene removal, three sizes of ceramic spheres with 0.008, 0.018, and 0.025 m in diameter served as packed materials, respectively. To maintain a constant operating temperature, the

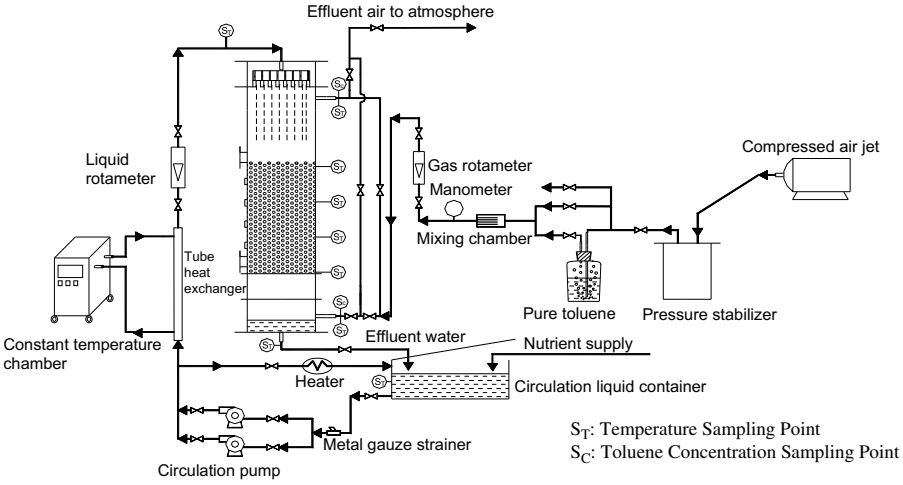

Fig. 2. Schematic of the experimental setup.

trickling biofilter was thermally insulated with polyurethane foam material with 0.02 m in thickness.

The experimental system consisted of air flow loop and liquid flow loop. Circulation liquid was delivered continuously from a circulation container into the liquid distributor at the top of the trickling biofilter by two circulation pumps for the nutrient feed, and then trickled down under gravity. The temperature in the trickling biofilter was justified by the heating capacity of heater and the cooling load of a constant temperature chamber installed in the circulation water loop. The exhaust water was drained into the circulation container from the bottom of the biofilter, finally. The air was inputted by an air compressor through a pressure stabilizer into a bottle with pure liquid toluene, and then the toluene exhaust gas was conveyed into the trickling biofilter from the bottom (the gas–liquid counter-current flow mode) or the top (the gas–liquid co-current flow mode). Finally, the treated gas exited from the outlet of the trickling biofilter to atmosphere.

The required measurements for the gas phase included the gas flow rate and the toluene concentration at the inlet and outlet of the trickling biofilter. The toluene concentration was measured by a gas chromatograph (GC) equipped with a flame ionization detector (FID) while the carrier gas (N_2) flow rate was set at 30 mL/min. The GC oven temperature and FID temperature were maintained at 80 °C and 170 °C, respectively. Liquid-phase samples were analyzed for the flow rate, absorbency ($OD_{600\,nm}$) and pH value. The analysis of $OD_{600\,nm}$ of the circulation liquid was carried out using a spectrophotometer, and the pH was measured by a pH meter calibrated with buffers (pH of 4.0 and 7.0) supplied by the manufacturer.

Before the start-up of the trickling biofilter, the circulation liquid in the container was seeded with an enriched aerobic microbial culture taken from an activated sludge system utilizing hydroxybenzene as one of the carbon sources. Then, the biofilm grew gradually on the surface of the packed materials while the toluene exhaust gas and the liquid replenished with fresh growth medium were circulated through the trickling biofilter. The medium solution was composed of the inorganic salts with a nitrogen-to-phosphorous ratio of 5:1 including 21.75 g $K_2HPO_4 \cdot H_2O$, 33.48 g $Na_2HPO_4 \cdot 12\,H_2O$, 5 g NH_4Cl, 8.5 g KH_2PO_4, 22.5 g $MgSO_4$, 36.4 g $CaCl_2$, 0.25 g $FeCl_3$, 0.04 g $MnSO_4 \cdot H_2O$, 0.04 g $InSO_4 \cdot H_2O$, and 0.03 g $(NH_4)_6Mo_7O_{24} \cdot 4H_2O$ per liter of deionized water, to grow microorganisms in an environment of carbon and energy source free for the biomass. Besides, Na_2HPO_4 was added into the solution as a pH buffer.

All experiments were performed with a circulation liquid flow rate (Q_l) from 0.009 to 0.0616 m^3/h, and a gas flow (Q_g) rate from 0.4 to 1.2 m^3/h at room temperature (about 27 °C) and each run under a given operating operation lasted for 24 h at least. Due to the significant effect of the liquid and gas flow arrangement on the biofilm distribution and the purification performance in the trickling biofilter, the start-up of the trickling biofilter with the ceramic spheres of 0.008 m in diameter was respectively carried out under the gas–liquid co-current flow mode and the gas–liquid counter-current flow mode, the trickling biofilter with ceramic spheres of 0.018 m in diameter under co-current flow mode, and the one with ceramic spheres of 0.025 m in diameter under counter-current flow mode. After each turn for waste gas purification experiment with a specific start-up completed, the trickling biofilter was necessarily rinsed and disinfected.

4. Parameters for model prediction

The purification performance of the trickling biofilter for purifying toluene exhaust was numerically calculated with the present model. The basic parameters used by the model are shown in Table 1 [17,22,23] for toluene exhaust treatment with the trickling biofilter. The relationship of the flow rates of gas and liquid in the capillary tube with the circulation liquid flow rate and the gas flow rate of the trickling biofilter can be expressed by Eqs. (52) and (53)

Table 1
Parameter values used for solving the model equation

Parameter	Value	Unit
$C_{gO,in}$	275×10^{-3}	g/m^3
D_{bO} [22]	1.54×10^{-9}	m^2/s
D_{bT} [17]	0.85×10^{-9}	m^2/s
D_{lO}	2.41×10^{-9}	m^2/s
D_{lT} [23]	1.03×10^{-9}	m^2/s
K_{IT} [23]	78.94	g/m^3
K_O	0.26	g/m^3
K_T [23]	11.03	g/m^3
m_O	34.4	
m_T [23]	0.27	
X_V [23]	100.0	kg/m^3
Y_O	0.341	kg/kg
Y_T [23]	0.708	kg/kg
μ_{max} [23]	1.5	h^{-1}

$$q_l = \frac{Q_l}{3600 n_c}, \tag{52}$$

$$q_g = \frac{Q_g}{3600 n_c}, \tag{53}$$

where $n_c = \frac{\varepsilon D_T^2}{4 r_s^2}$ is the number of capillary tubes in the trickling biofilter and D_T represents the diameter of the trickling biofilter (m).

As mentioned above, the correction factor, ξ, in Eq. (51) was determined by fitting the experimental data with the theoretical solution. The calculated results indicate that the ξ for the trickling biofilter packed with the ceramic spheres of 0.008 m in diameter under co-current flow mode and counter-current flow mode is 0.38 and 0.4, respectively. The value of ξ for 0.018 m ceramic spheres under co-current flow mode is 1.0, and the one for 0.025 m ceramic spheres under counter-current flow mode is 1.38.

5. Results and discussion

In this study, the purification performances of the trickling biofilter for toluene exhaust treatment were firstly predicted under the same operation conditions as the present experiments in order to verify the present model. And then, the effect of the various parameters such as the liquid and gas flow rate, the specific surface area of packed material, the porosity of packed bed, and the height of packed bed on purification efficiency were investigated respectively in virtue of the numerical simulations.

5.1. Comparison between experimental data and theoretical prediction

For verifying model, the model predictions are separately compared with the experimental results for toluene removal by the trickling biofilter with the ceramic spheres of 0.008 m, 0.018 m, and 0.025 m in diameter. The model predictions and experimental results at various liquid flow rates and gas flow rates under the co-current flow mode are shown in Figs. 3 and 4, and the results under the

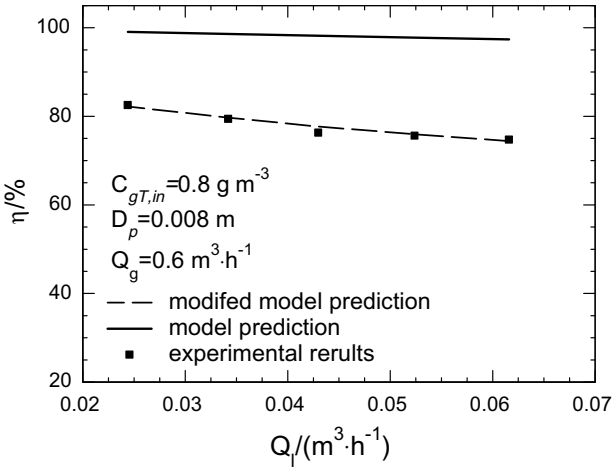

Fig. 3. Effect of liquid flow rate on purification efficiency of the trickling biofilter with ∅0.008 m ceramic spheres under the gas–liquid co-current flow mode.

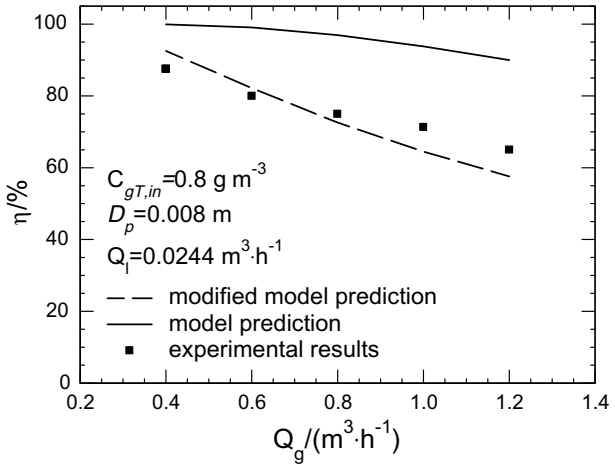

Fig. 4. Effect of gas flow rate on purification efficiency of the trickling biofilter with ∅0.008 m ceramic spheres under the gas–liquid co-current flow mode.

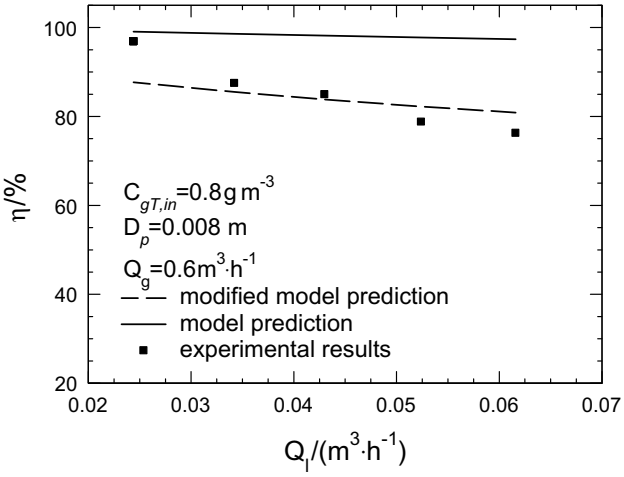

Fig. 5. Effect of liquid flow rate on purification efficiency of the trickling biofilter with ∅0.008 m ceramic spheres under the gas–liquid counter-current flow mode.

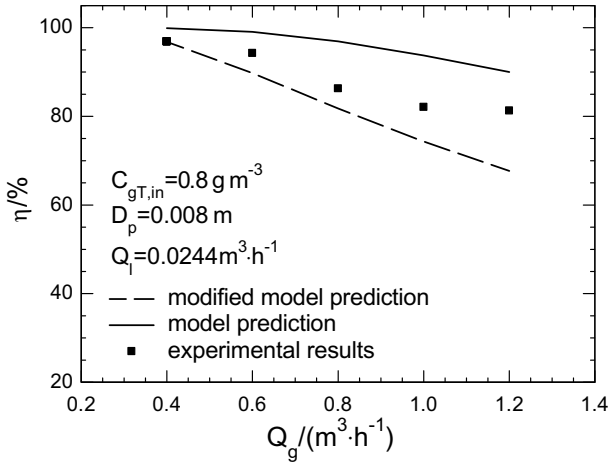

Fig. 6. Effect of gas flow rate on purification efficiency of the trickling biofilter with ∅0.008 m ceramic spheres under the gas–liquid counter-current flow mode.

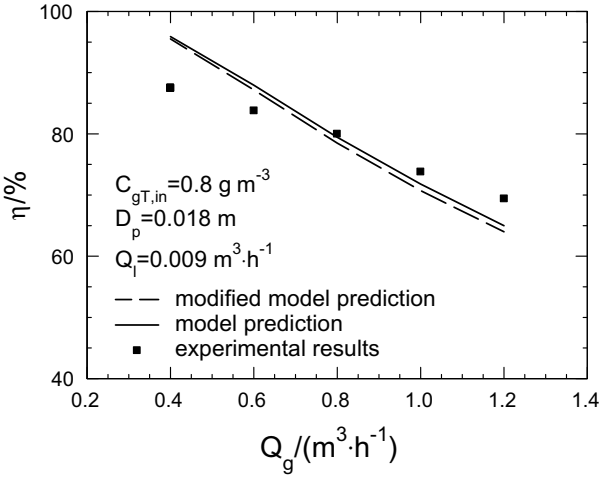

Fig. 8. Effect of gas flow rate on purification efficiency of the trickling biofilter with ∅0.018 m ceramic spheres under the gas–liquid co-current flow mode.

counter-current flow mode in Figs. 5 and 6. Both the numerical result with the total surface area of the packed materials and the one with the modified active biofilm area were shown in these figures. It can be seen that the model predicted values, especially using the specific wetted surface area of the biofilm, for the purification efficiency have a good agreement with the experimental data. The similar varying tendency of purification efficiency with the liquid flow rate and the gas flow rate can be found from the experimental results and the theoretical prediction. Figs. 3 and 4 show the variation of purification efficiency with the liquid flow rate and gas flow rate under co-current flow mode, where the discrepancies between the numerical prediction with the specific wetted surface area and the experimental data is less than 1.4% and 11.3%, respectively. Figs. 5 and 6 depict the variation of purification efficiency of the trickling biofilter with the liquid flow rate and gas flow rate under counter-current flow mode, which indicates the maximum discrepancy is 9.5% and 16.7%, respectively. Figs. 7 and 8 show the experimental results and theoretical predicted results of purification efficiency of the trickling biofilter packed with ceramic spheres of 0.018 m in diameter at different gas flow rates and liquid flow rates under co-current flow mode. It is indicated from these figures that the discrepancy between the theoretical predicted data and experimental data for purification efficiency is less than 6.3% and 9.5%, respectively. The modified model prediction and experimental results at various liquid and gas flow rates on the purification efficiency of the trickling biofilter with ceramic spheres of 0.025 m in diameter under the gas–liquid counter-current flow mode are shown in Figs. 9 and 10, where the maximum discrepancy is 3.3% and 30.9%, respectively. In the coming section, the effects of various key factors on the purification efficiency of the

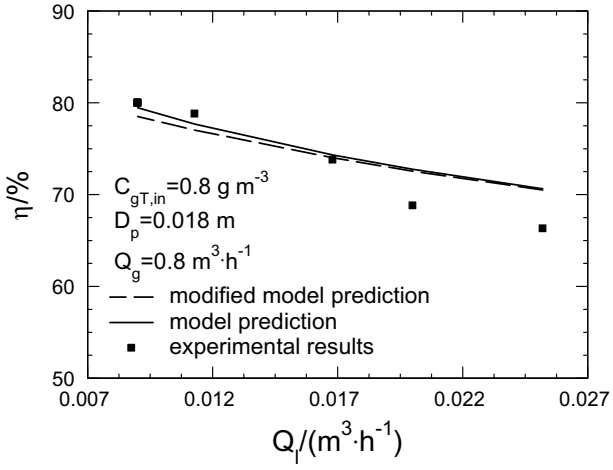

Fig. 7. Effect of liquid flow rate on purification efficiency of the trickling biofilter with ∅0.018 m ceramic spheres under the gas–liquid co-current flow mode.

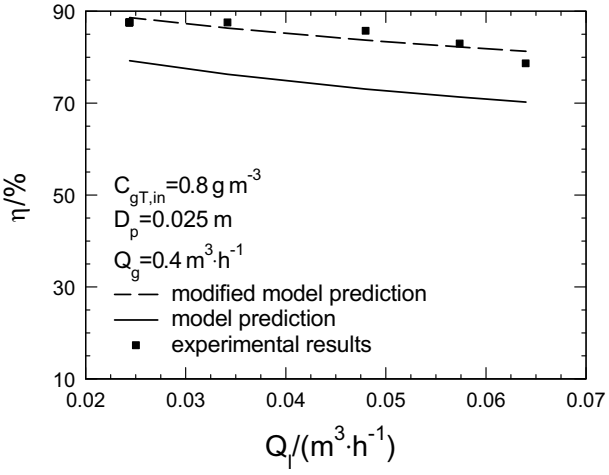

Fig. 9. Effect of liquid flow rate on purification efficiency of the trickling biofilter with ∅0.025 m ceramic spheres under the gas–liquid counter-current flow mode.

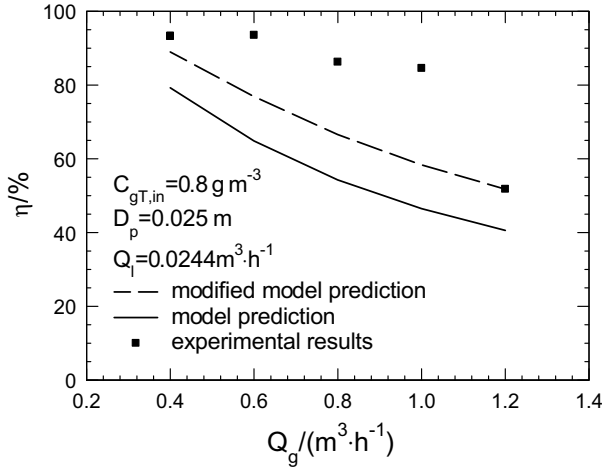

Fig. 10. Effect of gas flow rate on purification efficiency of the trickling biofilter with ∅0.025 m ceramic spheres under the gas–liquid counter-current flow mode.

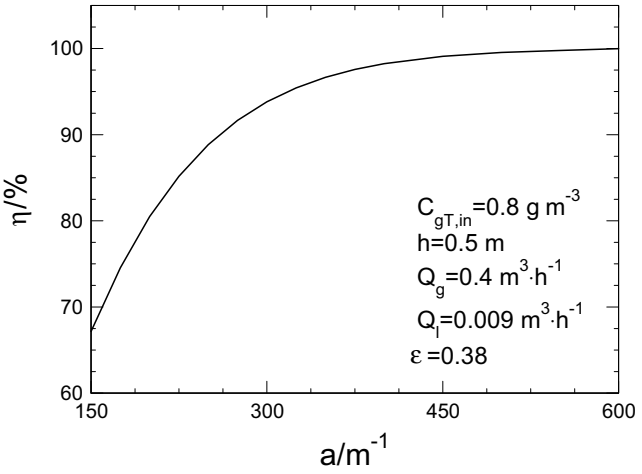

Fig. 11. Effect of specific surface area of packed material on purification efficiency of the trickling biofilter under the gas–liquid co-current flow mode.

trickling biofilter will be studied for the gas–liquid co-current flow mode in virtue of the theoretical predicted data.

5.2. Effect of the liquid and gas flow rate on the purification efficiency

It can be known from Figs. 3 and 5 that the purification efficiency decreases with the increase of the liquid flow rate at a fixed inlet toluene concentration and gas flow rate. This is mainly resulted from that a larger liquid flow rate induces a thicker liquid film over the biofilm with a larger pollutant mass transport resistance in the liquid film zone and thus, a less pollutant mass flux diffusing into the biofilm. In Figs. 4 and 6, we can see that the purification efficiency of trickling biofilter reduces with the gas flow rate increasing at a fixed liquid flow rate. This is mainly caused by the reason that under the specific liquid flow rate and inlet pollutant concentration, a larger gas flow rate leads to a larger pollutant mass flux and namely, a larger treatment load. As a result, the purification efficiency reduces with the increase in the gas flow rate.

5.3. Effect of the geometric parameters of the packed materials on the purification efficiency

Fig. 11 shows the effect of the specific surface area of the packed materials to the purification efficiency. We can see in this figure that the purification efficiency increases with the specific surface area of the packed material increasing. It can be explained by that a larger specific surface area of the packed material leads to a larger gas–liquid interface area, which results in a larger mass transport area and a thinner liquid film thickness over the biofilm and thus a larger mass flux from the gas core zone to the reaction zone. From Fig. 11, we can also see that at a larger specific surface area of the packed material, the increase in the specific surface area of the packed material has a less influence in the purification efficiency. It is due to the fact that the biochemical reaction becomes a limited factor as compared with the larger mass transport ability at a larger specific surface area.

Fig. 12 shows that the effect of the porosity of the packed bed on the purification efficiency. It is known that as the porosity of the packed bed increasing, the purification efficiency firstly increases to the largest one and then, decreases. This is mainly caused by the reason that at a fixed specific surface area of the packed material, as the porosity of the packed bed increasing, the flow cross-sectional area increases and accordingly, the practical gas flow rate in the pore of packed material decreases. As indicated in the former section, a smaller gas flow rate will induce larger purification efficiency. However, the increase in the porosity of packed bed can also lead to the decrease in the effective mass transport area and the increase in mass transport resistance, which results in the purification effi-

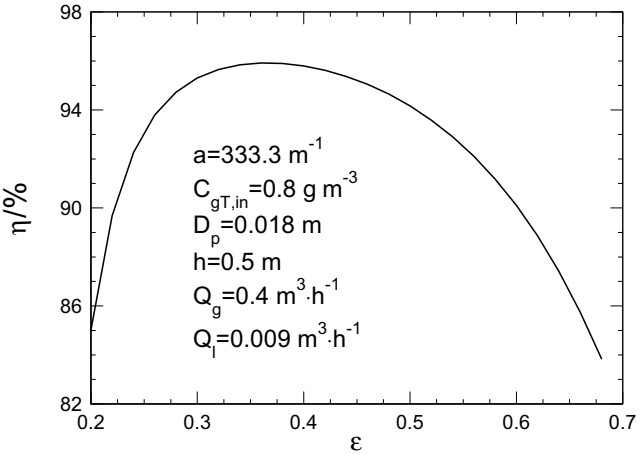

Fig. 12. Effect of porosity of packed bed on purification efficiency of the trickling biofilter under the gas–liquid co-current flow mode.

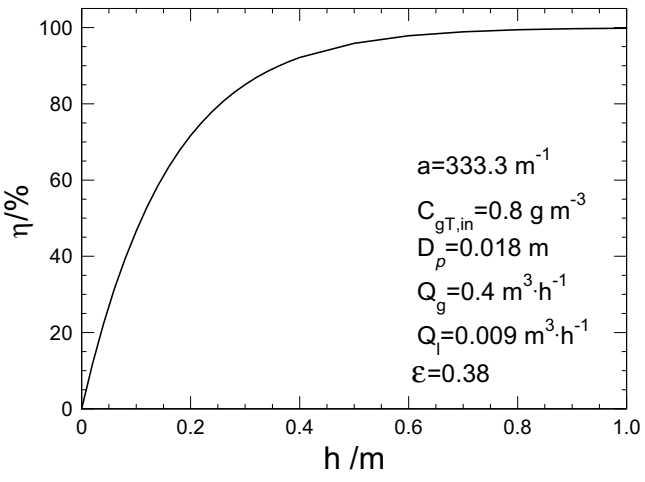

Fig. 13. Effect of the height of the packed bed on purification efficiency of the trickling biofilter under the gas–liquid co-current flow mode.

ciency reducing. As a result, there is an optimum porosity of the packed bed corresponding to the highest purification efficiency.

Fig. 13 shows the effect of the height of the packed bed on purification efficiency. It can be seen in this figure that with the increase in the height of the packed bed, the purification efficiency increases. The main reason is the fact that as the height of the packed bed increasing, the mass transport area is increasing, which leads to a larger mass transport flux and biodegradation. We can also see in this figure that the increase in the height of the packed bed causes comparatively sharper increase in the purification efficiency for a trickling biofilter with smaller height. As the height of the packed bed increasing, the rise of purification efficiency becomes gentler. This is mainly caused by the reason that as the height of the packed bed increasing, the local pollutant concentration becomes lower, which leads to a smaller pollutant mass transport from the gas core zone to the bioreaction zone in the biofilm and thus, the rise of purification efficiency reduces.

6. Conclusions

A mathematical model for predicting gas–liquid two-phase flow and a VOC waste gas degradation in a trickling biofilter is proposed in this paper. In this model, the packed bed is simplified into a series of straight capillary tubes covered by the biofilm and dividing the field of capillary tube into the gas core zone, the liquid film zone, and the biofilm zone. The effects of the pollutant absorption at the gas–liquid interface, the mass transport resistance in the liquid film zone and the biofilm zone, the biochemical reaction in the biofilm, and the limitation of oxygen to the bioreaction of microorganism have been incorporated in the model. The theoretical formula of the liquid film thickness in the capillary tube is derived by solving a set of momentum conservation equations for the liquid–gas co-current flow mode and counter-current flow mode. An iterative computation process is employed to solve the mass transport equations established for the gas core, the liquid film, and the biofilm. It has been showed that the predicted purification efficiencies for the low concentration toluene waste gas are favorably in an agreement with the experimental data. Based on the capillary tube model, the effects of the liquid and gas flow rate, the specific surface area of the packed material, the porosity of packed bed, and the height of the packed bed are studied, respectively. The following conclusions may be drawn from this study:

(1) With the increase in the liquid flow rate, the liquid film thickness is increased, which leads to a larger mass transport resistance in the liquid film and a lower purification efficiency.
(2) An increase in the waste gas flow rate leads to a reduction in the purification efficiency, which is caused by the increase in the pollutant loading.
(3) The purification efficiency increases with the increase in the height of packed bed.
(4) A lager specific surface area of the packed material causes larger purification efficiency. There exists an optimal porosity of the packed bed corresponding to the maximal purification efficiency of the trickling biofilter.

Acknowledgement

This work was supported by the National Natural Science Foundation of China (Grant No. 90510020, No. 50576107), NCET, and SRFDP.

References

[1] H.H.J. Cox, M.A. Deshusses, Biological waste air treatment in biotrickling filters, Curr. Opin. Biotechnol. 9 (1998) 256–262.
[2] C. Kennes, M.C. Veiga, Bioreactors for Waste Gas Treatment, Kluwer Academic Publishers, Dordrecht, 2001, pp. 99.
[3] S.P.P. Ottengraf, A.H.C. van den Oever, Kinetics of organic compound removal from waste gases with a biological filter, Biotechnol. Bioeng. XXV (1983) 3089–3102.
[4] D.S. Hodge, J.S. Devinny, Modeling removal of air pollutants by biofiltration, J. Environ. Eng. 121 (1) (1995) 21–33.
[5] M.A. Deshusses, G. Hamer, I.J. Dunn, Behavior of biofilters for waste air biotreatment. 1. Dynamic model development, Environ. Sci. Technol. 29 (4) (1995) 1048–1058.
[6] P. Viotti, B. Eramo, M.R. Boni, A. Carucci, M. Leccese, S. Sbaffoni, Development and calibration of a mathematical model for the simulation of the biofiltration process, Adv. Environ. Res. 7 (2002) 11–33.
[7] C.J. Mpanias, B.C. Baltzis, An experimental and modeling study on the removal of mono-chlorobenzene vapor in biotrickling filters, Biotechnol. Bioeng. 59 (3) (1998) 328–343.
[8] B.C. Baltzis, C.J. Mpanias, S. Bhattacharya, Modeling the removal of VOC mixtures in biotrickling filters, Biotechnol. Bioeng. 72 (4) (2001) 389–401.
[9] A.K. Sun, J. Hong, T.K. Wood, Modeling trichloroethylene degradation by a recombinant pseudomonad expressing toluene ortho-monooxygenase in a fixed-film bioreactor, Biotechnol. Bioeng. 59 (1) (1998) 40–51.

[10] R. Mirpuri, W. Sharp, et al., Predictive model for toluene degradation and microbial phenotypic profiles in flat plate vapor phase bioreactor, J. Environ. Eng. 123 (6) (1997) 586–592.
[11] C. Alonso, M.T. Suidan, B.R. Kim, B.J. Kim, Dynamical mathematical model for the biodegradation of VOCs in a biofilter: biomass accumulation study, Environ. Sci. Technol. 32 (20) (1998) 3118–3123.
[12] Q. Liao, R. Chen, X. Zhu, Theoretical model for removal of volatile organic compound (VOC) air pollutant in trickling biofilter, Sci. China (Series E) 46 (3) (2003) 245–258.
[13] C. Hammecker, L. Barbiéro, P. Boivin, J.L. Maeght, E.H.B. Diaw, A Geometrical pore model for estimating the microscopical pore geometry of soil with infiltration measurements, Transp. Porous Media 54 (2004) 193–219.
[14] T.S. Zhao, Q. Liao, Theoretical analysis of film condensation heat transfer inside vertical mini triangular channels, Int. J. Heat Mass Transfer 45 (13) (2002) 2829–2842.
[15] M. Kaviany, Principles of Heat Transfer in Porous Media, second ed., Springer-Verlag Publisher, New York, 1995, pp. 32–34.
[16] P.A. Jennings, Theoretical model for a submerged biological filter, Biotechnol. Bioeng. 18 (1976) 1249–1273.
[17] L. Bibeau, K. Kiared, A. Leroux, et al., Biological purification of exhaust air containing toluene vapor in a filter-bed reactor, Can. J. Chem. Eng. 75 (1997) 921–929.
[18] S.M. Zarook, B.C. Baltzis, Biofiltration of toluene vapor under steady-state and transient conditions: theory and experimental results, Chem. Eng. Sci. 49 (24) (1994) 4347–4360.
[19] R.M.M. Diks, S.P.P. Ottengraf, Verification studies of a simplified model for removal of dichloromethane from waste gases using a biological trickling filter (Part. I), Bioprocess Eng. 6 (1991) 93–99.
[20] R.M.M. Diks, S.P.P. Ottengraf, Verification studies of a simplified model for removal of dichloromethane from waste gases using a biological trickling filter (Part. II), Bioprocess Eng. 6 (1991) 131–140.
[21] A.R. Pedersen, E. Arvin, Removal of toluene in waste gases using a biological trickling filter, Biodegradation 6 (1995) 109–118.
[22] L.M. Freitas Dos Santos, A.G. Livingston, Novel membrane bioreactor for detoxification of VOC wastewater: biodegradation of 1,2-dichloroethane, Water Res. 29 (1) (1995) 171–194.
[23] Z. Shareefdeen, B.C. Baltzis, Biofiltration of toluene vapor under steady-state and transient conditions: theory and experimental results, Chem. Eng. Sci. 49 (24) (1994) 4347–4360.